Earthquake Engineering and Structural Dynamics, in press.

MULTIOBJECTIVE OPTIMAL STRUCTURAL CONTROL OF THE NOTRE DAME BUILDING MODEL BENCHMARK*

E. A. JOHNSON†, P. G. VOULGARIS‡, AND L. A. BERGMAN¤

Department of Aeronautical and Astronautical Engineering,
University of Illinois at Urbana-Champaign, Urbana, IL 61801, U.S.A.

SUMMARY

Reduced-order, multiobjective optimal controllers are developed for the Notre Dame structural control building model benchmark. Standard H_2/LQG optimal control excels at noise and disturbance rejection, but may have difficulty with actuator saturation and plant uncertainty. The benchmark problem is adapted to a multiobjective optimal control framework, using l_1 and H_∞ constraints to improve controller performance, especially attempting to reduce peak responses, avoid saturation, and improve robustness to unmodelled dynamics. The tradeoffs between H_2 performance, output peak magnitudes, and robust stability are examined. Several optimal controllers and their performance on the benchmark are given.

KEY WORDS: active structural control; earthquake response; multiobjective optimal control; H_∞ control; l_1 control

INTRODUCTION

Spencer *et al.*[1,2] detailed a building model benchmark problem for studying active structural control strategies. The problem defines a base plant that models the structural behavior of a three-story, single-bay, scale model of a building[3], as well as the dynamics of the sensors (an LVDT, several accelerometers, and a force transducer) and the actuator (an active mass driver or an active tendon member). Such a benchmark problem is invaluable for studying various control strategies with realistic limitations such as actuator saturation, limited actuator stroke, digital controller implementation, reduced-order controllers, and multiple measures of controller performance and robustness.

Standard H_2/LQG optimal control design methods typically excel at noise and disturbance rejection, but may have difficulty with actuator saturation and plant uncertainty. The addition of l_1 constraints may help accommodate requirements such as limiting control output or other peak

*This paper is dedicated to Franz Ziegler, Professor of Rational Mechanics and Head of the *Institut für Allgemeine Mechanik* at the Vienna University of Technology, on the occasion of his 60th birthday.

†Formerly, Graduate Research Assistant; currently, Visiting Research Assistant Professor, Department of Civil Engineering and Geological Sciences, University of Notre Dame, Notre Dame, IN 46556; e-mail: johnsone@nd.edu

‡Associate Professor; e-mail: petros@control.csl.uiuc.edu

¤Professor; e-mail: lbergman@uiuc.edu

measures of system performance. Furthermore, H_∞ robust control design methods are advantageous since the model of a plant always contains some measure of uncertainty for any real-world application, whether due to modelling errors or long-term changes in system dynamics. With a small sacrifice in the system H_2 norm from that found using an H_2 (LQG) optimal controller, giving slightly larger root mean square response to white noise excitation, the l_1 and H_∞ norms can often be significantly reduced, leading to better performance and more robust stability. The use of all three of these norms to devise an optimal controller can combine the strengths of each.

The general formulation of the mixed H_2/H_∞ optimal control design problem has been explored in a number papers (*e.g.*, Khargonekar and Rotea[4], Kaminer *et al.*[5], Bernstein and Haddad[6]), building on H_2 and H_∞ control methods in Doyle *et al.*[7-9] The l_1 optimal control problem has also been detailed in various papers and texts (*e.g.*, Dahleh and Pearson[10]; Dahleh and Diaz-Bobillo[11]; Khammash[12]). A number of solution methods have been developed to solve certain mixed-norm control design problems (*e.g.*, Whorton *et al.*[13], Voulgaris[14]). For example, the homotopy algorithm of Whorton *et al.*[13] uses a linear combination of the objective H_2 and H_∞ norms, varying the ratio of the linear coefficients and searching incrementally in the H_2 and H_∞ directions to define a family of mixed-norm designs.

To facilitate numerical solutions to general mixed-norm optimal control problems, Jacques, Canfield, Ridgely, and Spillman[15-19] developed a set of numerical algorithms and accompanying MATLAB® code to search for fixed-order controllers that minimize an H_2 norm while constraining one or more H_2, l_1 (or L_1), and H_∞ norms below some critical values. These algorithms, which can be used for continuous- or discrete-time systems, have been adapted to the current problem with alteration of the associated software.

BENCHMARK PROBLEM REQUIREMENTS

The base plant[1,2] is described by the block diagram in Fig. 1 and by the state equations

$$\begin{aligned} \dot{\mathbf{x}} &= \mathbf{A}\mathbf{x} + \mathbf{B}u + \mathbf{E}\ddot{x}_g \\ \mathbf{z} &= \mathbf{C}_z\mathbf{x} + \mathbf{D}_z u + \mathbf{F}_z\ddot{x}_g \\ \mathbf{y} &= \mathbf{C}_y\mathbf{x} + \mathbf{D}_y u + \mathbf{F}_y\ddot{x}_g + \mathbf{v} \end{aligned} \qquad \mathbf{z} = \left\{ \begin{array}{c} [\,x_1 \;\; x_2 \;\; x_3 \;\; x_m\,]^{\mathrm{T}} \\ [\,\dot{x}_1 \;\; \dot{x}_2 \;\; \dot{x}_3 \;\; \dot{x}_m\,]^{\mathrm{T}} \\ [\,\ddot{x}_1^a \;\; \ddot{x}_2^a \;\; \ddot{x}_3^a \;\; \ddot{x}_m^a\,]^{\mathrm{T}} \end{array} \right\} \quad \mathbf{y} = \mathbf{v} + \left[x_m \;\; \ddot{x}_1^a \;\; \ddot{x}_2^a \;\; \ddot{x}_3^a \;\; \ddot{x}_m^a \;\; \ddot{x}_g \right]^{\mathrm{T}} \quad (1)$$

where $\mathbf{x}$ is the state vector (in $\Re^{28}$ for the active mass driver (AMD) system and in $\Re^{20}$ for the active tendon system (TEN)), $\mathbf{y}$ is the measurement vector, $\mathbf{z}$ is a vector of responses to be regu-

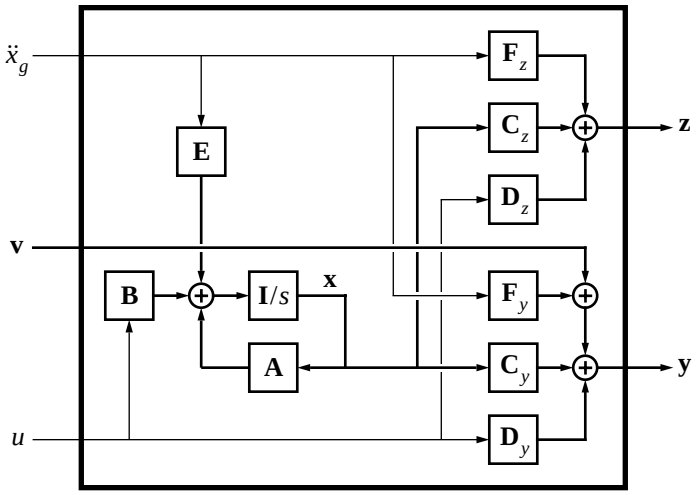

Figure 1. Block diagram of benchmark plant.

lated, u is the actuator input, $\ddot{x}_g$ is the seismically-induced ground acceleration, and $\mathbf{v}$ is the sensor noise (independent, zero-mean, Gaussian white noise processes). The components of the output measurement $\mathbf{y}$ and regulated response $\mathbf{z}$, the former corrupted by sensor noise, include the displacement x_i and velocity $\dot{x}_i$ of the i^{th} floor relative to the ground, absolute accelerations of the i^{th} floor $\ddot{x}_i^a$ and the ground $\ddot{x}_g$, relative actuator displacement x_m and velocity $\dot{x}_m$, and either the active mass absolute acceleration $\ddot{x}_m^a$ or the active tendon force f. In the active tendon system, the tendon force f replaces the active mass acceleration $\ddot{x}_m^a$ in both $\mathbf{y}$ and $\mathbf{z}$ in (1). Interstory drifts are defined as $d_1(t) = x_1(t)$, $d_2(t) = x_2(t) - x_1(t)$, and $d_3(t) = x_3(t) - x_2(t)$.

The coefficient matrices in (1) represent the input-output behavior of the building models in the Notre Dame Structural Dynamics and Control / Earthquake Engineering Laboratory (SDC/EEL) up to 100Hz (the AMD system) and the National Center for Earthquake Engineering Research (NCEER) up to 50Hz (the TEN system). Both sets of coefficient matrices were distributed in a MATLAB® MAT-file as a part of the benchmark problem definition.[20]

The goal, then, is to design a stable, discrete-time controller with sampling period $T = 1$ ms, subject to several implementation constraints:

(*a*) the sensor noise components are Gaussian rectangular pulse processes of 1 ms duration and root mean square magnitude 0.01 V.

(*b*) the A/D and D/A converters at the controller input and output have 12-bit precision and a span of ± 3V;

(*c*) the controller may have no more than 12 states; and

(*d*) the resulting actuator response must be within the bounds of the 6 hard constraints, $C_i \le 1$, $1 \le i \le 6$, as defined below.

The performance of the controller is then judged by 10 performance measures, J_i, $1 \le i \le 10$, as summarized below.

RMS Responses to Kanai-Tajimi Excitation Spectrum

The first five performance measures are root mean square responses to a family of Kanai-Tajimi excitation spectra.[21] The two-sided spectral density $S_{\ddot{x}_g \ddot{x}_g}(\omega)$ is given by

$$S_{\ddot{x}_g \ddot{x}_g}(\omega) = S_0 \frac{4\zeta_g^2 \omega_g^2 \omega^2 + \omega_g^4}{(\omega^2 - \omega_g^2)^2 + 4\zeta_g^2 \omega_g^2 \omega^2} \qquad S_0 = \frac{s_0 \zeta_g}{\pi \omega_g (4\zeta_g^2 + 1)} \tag{2}$$

where the frequency ω_g and damping ratio ζ_g of the bedrock-ground connection are in given ranges ($\zeta_g \in [0.3, 0.75]$, ω_g as per Table I). (The intensity of the excitation is such that $\sigma_{\ddot{x}_g}$, the root mean square ground acceleration, is given in Table I and is independent of ω_g and ζ_g.) The performance measures, weighted by the nondimensionalization parameters j_i in Table I, are root mean square structural response (maximum interstory drifts and maximum floor acceleration) and actuator response (actuator displacement, velocity, and acceleration or force), defined by

$$J_1 = \max_{\omega_g, \zeta_g, i} \frac{\sigma_{d_i}}{j_1} \qquad J_2 = \max_{\omega_g, \zeta_g, i} \frac{\sigma_{\ddot{x}_i^a}}{j_2} \qquad J_3 = \max_{\omega_g, \zeta_g} \frac{\sigma_{x_m}}{j_3} \tag{3}$$

$$J_4 = \max_{\omega_g, \zeta_g} \frac{\sigma_{\dot{x}_m}}{j_4} \qquad J_5 = \max_{\omega_g, \zeta_g} \frac{\sigma_{\ddot{x}_m^a} \text{ or } \sigma_f}{j_5} \tag{4}$$

with the constraints

$$C_1 = \max_{\omega_g, \zeta_g} \frac{\sigma_u}{\sigma_u^{\text{MAX}}} \le 1 \qquad C_2 = \max_{\omega_g, \zeta_g} \left[\frac{\sigma_{\ddot{x}_m^a}}{\sigma_{\ddot{x}_m^a}^{\text{MAX}}} \text{ or } \frac{\sigma_f}{\sigma_f^{\text{MAX}}} \right] \le 1 \qquad C_3 = \max_{\omega_g, \zeta_g} \frac{\sigma_{x_m}}{\sigma_{x_m}^{\text{MAX}}} \le 1 \tag{5}$$

where σ_u^{MAX}=1V, $\sigma_{\ddot{x}_m^a}^{\text{MAX}}$=$2g$, σ_f^{MAX}=4kN, and $g = 9.8\text{m/s}^2$. RMS responses are computed via a SIMULINK® block similar to that in Spencer *et al.*[1,2] up to 300 (AMD) or 750 (TEN) seconds.

Table I. Performance measure normalization parameters and benchmark constants.

actu-ator	s_0	ω_g	$\sigma_{\ddot{x}_g}$	$\sigma_{x_m}^{\text{MAX}}$	x_m^{MAX}	j_1	j_2	j_3	j_4	j_5	j_6	j_7	j_8	j_9	j_{10}	earth-quake
AMD	0.03 V^2	[20,120] $\frac{\text{rads}}{\text{sec}}$	0.12 g	3 cm	9 cm	1.31 cm	1.79 g	1.31 cm	47.9 $\frac{\text{cm}}{\text{sec}}$	1.79 g	3.37 cm	5.05 g	3.37 cm	131 $\frac{\text{cm}}{\text{sec}}$	5.05 g	El Centro
											1.66 cm	2.58 g	1.66 cm	58.3 $\frac{\text{cm}}{\text{sec}}$	2.58 g	Hachinohe
TEN	587.5 $(\text{mV})^2$	[8,50] $\frac{\text{rads}}{\text{sec}}$	0.034 g	1 cm	3 cm	2.34 cm	0.485 g	2.34 cm	33.3 $\frac{\text{cm}}{\text{sec}}$	289 kN	6.45 cm	1.57 g	6.45 cm	99.9 $\frac{\text{cm}}{\text{sec}}$	289 kN	El Centro
											3.78 cm	0.778 g	3.78 cm	56.1 $\frac{\text{cm}}{\text{sec}}$		Hachinohe

Peak Responses to NS Records of the 1940 El Centro and 1968 Hachinohe Earthquakes

The remaining five performance measures are peak responses to the scaled ground acceleration records of two actual earthquakes. (The records and appropriate scaling were defined in the benchmark.[20]) The performance measures are

$$J_6 = \max_{\substack{t,\,i \\ \text{El Centro} \\ \text{Hachinohe}}} \frac{|d_i(t)|}{j_6} \qquad J_7 = \max_{\substack{t,\,i \\ \text{El Centro} \\ \text{Hachinohe}}} \frac{|\ddot{x}_i^a(t)|}{j_7} \qquad J_8 = \max_{\substack{t \\ \text{El Centro} \\ \text{Hachinohe}}} \frac{|x_m(t)|}{j_8} \tag{6}$$

$$J_9 = \max_{\substack{t \\ \text{El Centro} \\ \text{Hachinohe}}} \frac{|\dot{x}_m(t)|}{j_9} \qquad J_{10} = \max_{\substack{t \\ \text{El Centro} \\ \text{Hachinohe}}} \frac{|\ddot{x}_m^a(t) \text{ or } f(t)|}{j_{10}} \tag{7}$$

with constraints

$$C_4 = \max_{\substack{t \\ \text{El Centro} \\ \text{Hachinohe}}} \frac{|u(t)|}{u^{\text{MAX}}} \le 1 \qquad C_5 = \max_{\substack{t \\ \text{El Centro} \\ \text{Hachinohe}}} \left[\frac{|\ddot{x}_m^a(t)|}{\ddot{x}_m^{a\text{MAX}}} \text{ or } \frac{f(t)}{f^{\text{MAX}}} \right] \le 1 \qquad C_6 = \max_{\substack{t \\ \text{El Centro} \\ \text{Hachinohe}}} \frac{|x_m(t)|}{x_m^{\text{MAX}}} \le 1 \tag{8}$$

where $u^{\text{MAX}}=3\text{V}$, $\ddot{x}_m^{a\text{MAX}}=6g$, and $f^{\text{MAX}}=12\text{kN}$.

Performance of a "Sample" LQG Controller for the Active Mass Driver System

One "sample" controller, based on an LQG design that weights the three floor accelerations equally and feeds back the accelerations of the three floors and the active mass, was computed by Spencer *et al.*[1]; the resulting values of the performance measures are given in Table II.

Table II. Performance of sample LQG controller on the AMD system.

J_1	J_2	J_3	J_4	J_5	J_6	J_7	J_8	J_9	J_{10}	C_1	C_2	C_3	C_4	C_5	C_6
0.283	0.440	0.510	0.513	0.628	0.456	0.711	0.670	0.775	1.34	0.143	0.56	0.224	0.175	0.605	0.222

NOTATION AND MATHEMATICAL DEFINITIONS

Various signal and system norms are used in formulating the multiobjective optimization problem to solve for mixed-norm optimal controllers. A brief mathematical description of these norms and their use in the current problem are as follows.

Let $\mathbf{x}(t)$ be a real-valued vector process in $\Re^m$, with its discrete-time correspondent, $\underset{\sim}{\mathbf{x}}(k)$, with sampling time T. The p-norm of this signal may be defined as

$$\|\mathbf{x}\|_p = \left[\int_{-\infty}^{\infty} \sum_{i=1}^{m} |x_i(t)|^p dt \right]^{1/p} \qquad \|\underset{\sim}{\mathbf{x}}\|_p = \left[T \sum_{k=-\infty}^{\infty} \sum_{i=1}^{m} |\underset{\sim}{x}_i(k)|^p \right]^{1/p} \tag{9}$$

The special cases for the 1-, 2-, and ∞-norms are

$$\begin{aligned} \|\mathbf{x}\|_1 &= \int_{-\infty}^{\infty} \sum_{i=1}^{m} |x_i(t)| dt & \|\underset{\sim}{\mathbf{x}}\|_1 &= T \sum_{k=-\infty}^{\infty} \sum_{i=1}^{m} |\underset{\sim}{x}_i(k)| \\ \|\mathbf{x}\|_2^2 &= \int_{-\infty}^{\infty} \mathbf{x}^*(t)\mathbf{x}(t) dt & \|\underset{\sim}{\mathbf{x}}\|_2^2 &= T \sum_{k=-\infty}^{\infty} \underset{\sim}{\mathbf{x}}^*(k)\underset{\sim}{\mathbf{x}}(k) \\ \|\mathbf{x}\|_\infty &= \sup_t \max_i |x_i(t)| & \|\underset{\sim}{\mathbf{x}}\|_\infty &= \sup_k \max_i |\underset{\sim}{x}_i(k)| \end{aligned} \tag{10}$$

where $(\,)^*$ denotes complex-conjugate transpose. (The sampling time is included in the discrete-time signal norms so that, assuming T is sufficiently small, the resulting norms are equivalent to that of the continuous-time signal.) A continuous-time signal is in L_p (a Lebesque space), or a discrete-time signal in l_p, if its p-norm is finite.

Let $\mathbf{G}(s)$ and $\underset{\sim}{\mathbf{G}}(z)$ denote the continuous- and discrete-time transfer functions of a system, respectively, with corresponding impulse response functions, $\hat{\mathbf{G}}(t)$ and $\hat{\underset{\sim}{\mathbf{G}}}(k)$. Furthermore, let $\mathbf{u}$ and $\mathbf{y}$ be excitation and response (input and output of the system), respectively. Then several key norms may be written as ($\bar{\sigma}[\,]$ denotes the largest singular value)

$$\begin{aligned} L_1\text{:}\quad & \|\mathbf{G}\|_1 = \max_i \int_{-\infty}^{\infty} \sum_{j=1}^{n} |\hat{g}_{ij}(t)| dt & l_1\text{:}\quad & \|\underset{\sim}{\mathbf{G}}\|_1 = \max_i \sum_{k=-\infty}^{\infty} \sum_{j=1}^{n} |\hat{\underset{\sim}{g}}_{ij}(k)| \\ H_2\text{:}\quad & \|\mathbf{G}\|_2^2 = \frac{1}{2\pi} \int_{-\infty}^{\infty} \text{trace}\,[\mathbf{G}^*(j\omega)\mathbf{G}(j\omega)]\, d\omega & H_2\text{:}\quad & \|\underset{\sim}{\mathbf{G}}\|_2^2 = \frac{1}{2\pi T} \int_{-\pi}^{\pi} \text{trace}\,[\underset{\sim}{\mathbf{G}}^*(e^{j\omega})\underset{\sim}{\mathbf{G}}(e^{j\omega})]\, d\omega \\ H_\infty\text{:}\quad & \|\mathbf{G}\|_\infty = \sup_\omega \bar{\sigma}[\mathbf{G}(j\omega)] & H_\infty\text{:}\quad & \|\underset{\sim}{\mathbf{G}}\|_\infty = \sup_\omega \bar{\sigma}[\underset{\sim}{\mathbf{G}}(e^{j\omega})] \end{aligned} \tag{11}$$

The H_2 norm of a system reflects the root mean square response to Gaussian white noise excitation, and thus it is central to control design for the benchmark problem; minimizing the closed loop H_2 norm $\|\mathbf{G}\|_2$ will minimize the root mean square output $\|\mathbf{y}\|_2$. The H_∞ norm is a worst-case magnification of excitation "energy" into the system response (*i.e.*, $\|\mathbf{G}\|_\infty = \max_{\mathbf{u} \in l_2} \|\mathbf{y}\|_2 / \|\mathbf{u}\|_2$); it also can be used to measure the worst-case sensitivity of the stability of the closed-loop system to unmodelled dynamics, such as high-frequency modes that are often neglected or have low signal-

to-noise ratios (making them difficult to model accurately). Thus, to minimize the H_∞ norm around an unknown block of unmodelled dynamics for robust control design will minimize the sensitivity of the closed-loop stability to the uncertainties in the model. Finally, the L_1 norm (or the l_1 norm for discrete-time systems), is the worst-case magnification of input magnitude; minimizing the L_1 norm can often decrease peak responses.

MULTIOBJECTIVE OPTIMAL CONTROL

The Mixed-Norm Toolbox[18,19], also known as MXTOOLS, is designed to solve mixed-norm, fixed-order, optimal control problems by choosing a controller of a selected order to minimize an H_2 norm subject to one or more H_2, L_1 or l_1, and H_∞ norm constraints. Assuming a base H_2 problem, one L_1 or l_1 constraint, and one H_∞ constraint, the problem is described by the the interrelated systems in Fig. 2 and the corresponding continuous-time state-space descriptions

$$\begin{aligned}
\dot{\mathbf{x}}_2 &= \mathbf{A}_2\mathbf{x}_2 + \mathbf{B}_\mathbf{w}\,\mathbf{w} + \mathbf{B}_2\,\mathbf{u} & \dot{\mathbf{x}}_1 &= \mathbf{A}_1\,\mathbf{x}_1 + \mathbf{B}_\mathbf{r}\,\mathbf{r} + \mathbf{B}_1\,\mathbf{u} & \dot{\mathbf{x}}_\infty &= \mathbf{A}_\infty\mathbf{x}_\infty + \mathbf{B}_\mathbf{d}\,\mathbf{d} + \mathbf{B}_\infty\,\mathbf{u} \\
\bar{\mathbf{z}} &= \mathbf{C}_{\bar{\mathbf{z}}}\mathbf{x}_2 + \mathbf{D}_{\bar{\mathbf{z}}\mathbf{w}}\mathbf{w} + \mathbf{D}_{\bar{\mathbf{z}}\mathbf{u}}\mathbf{u} & \mathbf{m} &= \mathbf{C}_\mathbf{m}\mathbf{x}_1 + \mathbf{D}_\mathbf{mr}\mathbf{r} + \mathbf{D}_\mathbf{mu}\mathbf{u} & \mathbf{e} &= \mathbf{C}_\mathbf{e}\,\mathbf{x}_\infty + \mathbf{D}_\mathbf{ed}\mathbf{d} + \mathbf{D}_\mathbf{eu}\mathbf{u} \\
\mathbf{y}_2 &= \mathbf{C}_2\mathbf{x}_2 + \mathbf{D}_\mathbf{yw}\mathbf{w} + \mathbf{D}_\mathbf{yu}\mathbf{u} & \mathbf{y}_1 &= \mathbf{C}_1\,\mathbf{x}_1 + \mathbf{D}_\mathbf{yr}\,\mathbf{r} + \mathbf{D}_\mathbf{yu}\,\mathbf{u} & \mathbf{y}_\infty &= \mathbf{C}_\infty\mathbf{x}_\infty + \mathbf{D}_\mathbf{yd}\mathbf{d} + \mathbf{D}_\mathbf{yu}\mathbf{u}
\end{aligned} \tag{12}$$

(or similar discrete-time equations), where state vectors $\mathbf{x}_2$, $\mathbf{x}_1$, and $\mathbf{x}_\infty$ may have some or all states in common and the measurements $\mathbf{y}_2$, $\mathbf{y}_1$, and $\mathbf{y}_\infty$ are equal in the absence of disturbances $\mathbf{w}$, $\mathbf{r}$, and $\mathbf{d}$, *i.e.*, $\mathbf{C}_2\mathbf{x}_2 = \mathbf{C}_1\mathbf{x}_1 = \mathbf{C}_\infty\mathbf{x}_\infty$. The input $\mathbf{w}$ is a zero-mean Gaussian white noise of unit intensity (*i.e.*, $E[\mathbf{w}(t)\mathbf{w}^{\mathrm{T}}(s)] = \mathbf{I}\delta(t-s)$ or $E[\mathbf{w}(k)\mathbf{w}^{\mathrm{T}}(l)] = \frac{1}{T}\mathbf{I}\delta_{kl}$, where T is the sampling period), the input $\mathbf{r}$ is assumed to be an unknown magnitude-bounded signal with $\|\mathbf{r}\|_\infty \le 1$, and the input $\mathbf{d}$ is assumed to be an unknown energy-bounded signal with $\|\mathbf{d}\|_2 \le 1$. No relationships are assumed between $\mathbf{w}$, $\mathbf{r}$, and $\mathbf{d}$ or between $\bar{\mathbf{z}}$, $\mathbf{m}$, and $\mathbf{e}$.

The $H_2/L_1/H_\infty$ (or $H_2/l_1/H_\infty$) optimization problem is then to find an admissible, stabilizing controller $\mathbf{K}$, with state space description ($\mathbf{A}_c$, $\mathbf{B}_c$, $\mathbf{C}_c$, $\mathbf{D}_c$), of a fixed order, that achieves

$$\inf_{\mathbf{K}\ \text{admissible}} \|\mathbf{T}_{\bar{\mathbf{z}}\mathbf{w}}\|_2 \quad \text{subject to} \quad \|\mathbf{T}_\mathbf{mr}\|_1 \le \nu \text{ and } \|\mathbf{T}_\mathbf{ed}\|_\infty \le \gamma \tag{13}$$

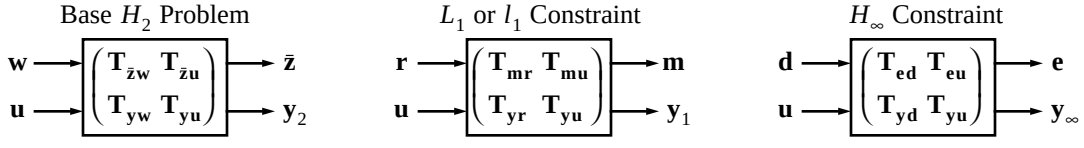

Figure 2. MXTOOLS plant with a base H_2 system, an L_1 or l_1 constraint, and an H_∞ constraint.

The requirements for solution with the fixed order at least that of the base H_2 subproblem are

- the base H_2 subproblem must have $(\mathbf{A}_2, \mathbf{B}_2)$ stabilizable and $(\mathbf{A}_2, \mathbf{C}_2)$ detectable,
- the base H_2 subproblem must be well posed, *i.e.*, $(\mathbf{I} + \mathbf{D}_c\mathbf{D}_{\mathbf{yu}})$ is invertible,
- the overall problem must be non-singular, and
- for continuous-time systems, $\mathbf{D}_{\mathbf{zw}} + \mathbf{D}_{\mathbf{zu}}\mathbf{D}_c\mathbf{D}_{\mathbf{yw}} = 0$ so that $\|\mathbf{T}_{\mathbf{zw}}\|_2$ is finite.

For a controller of lesser order, an additional requirement is the existence of a stabilizing controller of the given order that satisfies the constraints.

MXTOOLS parameterizes the controller in modal form to reduce the number of design variables (generally disallows repeated controller eigenvalues; one could modify MXTOOLS to use a full state-space, or any other, parameterization if repeated eigenvalues are thought to be required). The objective function, the constraints, and their gradients, are constructed[17] and passed to any constrained optimization algorithm. The default solver uses a sequential quadratic programming (SQP) method similar in function to MATLAB's Optimization Toolbox[22] `constr` function, but handles larger problems more effectively (`constr` often has difficulty maintaining a positive definite approximation to the Lagrangian Hessian for problems with more than 40 or 50 design variables).

The formulation above assumes one L_1 or l_1 constraint and one H_∞ constraint. Similar formulations for an arbitrary number of constraints may be performed. The current implementation of MXTOOLS is limited to one MIMO L_1 or l_1 constraint, though this is of no difficulty since several L_1 or l_1 constraints can be combined into one with appropriate scaling.

A few caveats in the use of MXTOOLS must be noted. First, no information is available as to how distant a computed fixed-order solution is from the true optimal, order-free solution.[19] For the benchmark problem, this is not of great concern since the controller order is restricted. Second, the search for reduced-order controllers may be more susceptible to the problem of local minima, but may be significantly easier to solve due to the reduced search space dimension.[19] Third, the l_1 norm tends to be quite conservative for most magnitude-bounded, but otherwise unknown, inputs, and therefore its values ought to be regarded in a relative, qualitative sense, rather than a measure of the actual performance on magnitude-bounded output constraints.[17]

The MXTOOLS software was a useful tool in solving the multiobjective problems in this study, though a fair amount of "tweaking" and a few bug fixes were necessary in the process.

FORMULATION OF THE SUBPROBLEMS

The benchmark problem can be augmented by various static and dynamic weights to transform it into a form suitable for a mixed-norm optimal controller search. One aspect of the benchmark problem rather indirectly addressed in the control design here is the 200 μs computational delay at the plant input (time to compute the control action and perform the A/D and D/A conversions); it is included here only in the H_∞ subproblem as a part of the plant uncertainty. If the delay were larger or considered more important, the base plant could be explicitly augmented from the start (at the plant input) with a Padé approximation of the delay.[23]

Some of the formulation given below is in continuous-time terms, but all such transfer functions were converted to discrete-time for the control optimization problem.

Base H_2 Problem

The base H_2 problem can be formulated by adding to the base plant various weighting functions for normalization, as shown in Fig. 3, where $\mathbf{w}$ is a 7×1 vector of zero-mean, Gaussian white noises with $E\,[\mathbf{w}(t)\mathbf{w}^{\mathrm{T}}(t+\tau)] = \mathbf{I}\delta(\tau)$. One element, or channel, of $\mathbf{w}$ is filtered through the second-order system $W_{\mathrm{KT}}(s)$ to model the Kanai-Tajimi spectrum

$$W_{\mathrm{KT}}(s,\, \omega_g,\, \zeta_g) = \sqrt{2\pi S_0}\ \frac{2\zeta_g\omega_g s + \omega_g^2}{s^2 + 2\zeta_g\omega_g s + \omega_g^2} \tag{14}$$

using the ground parameters ω_g and ζ_g that cause the worst uncontrolled response ($\zeta_g^{\mathrm{worst}} = 0.3$; $\omega_g^{\mathrm{worst}} = 37.28\frac{\mathrm{rads}}{\mathrm{sec}}$ for the active mass driver system and $\omega_g^{\mathrm{worst}} = 14.5\frac{\mathrm{rads}}{\mathrm{sec}}$ for the active tendon system). The remaining elements of $\mathbf{w}$ are weighted to model the sensor noise. At the output side, $W_{\bar{\mathbf{z}}u}$ is a weight on the control effort and W_u is a normalization factor. $\mathbf{M}_{\bar{\mathbf{z}}\mathbf{z}}$ is a matrix used to rearrange the outputs of the base plant into the elements to be regulated; $\mathbf{Z}_{\mathrm{V}}^{-1}$ converts from Volts to the dimensional units and then $\mathbf{J}_{1\text{-}5}^{-1}$ nondimensionalizes. $\mathbf{W}_{\bar{\mathbf{z}}}$ is a diagonal matrix to weight the normalized criteria differently as required for improved controller performance (the

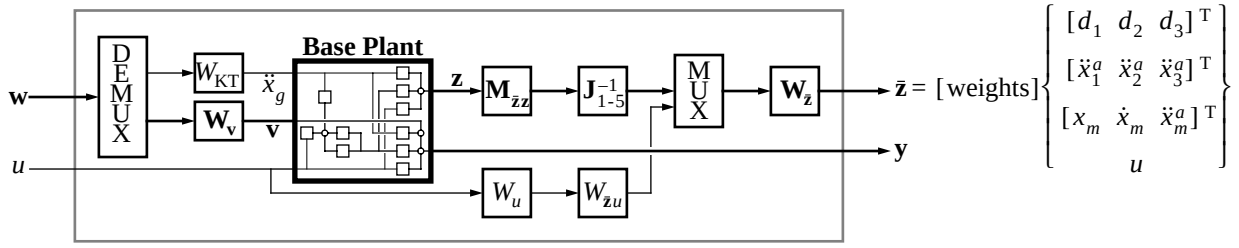

Figure 3. Block diagram of the base H_2 problem. (Note: "DEMUX" is a demultiplexer that separates two sets of signals in a multi-signal line; "MUX", or multiplexer, combines several channels into one vector signal.)

identity matrix was found acceptable in the final designs herein). The resulting output vector $\bar{\mathbf{z}}$ contains weighted forms of the three interstory drifts, the three floor accelerations, and the actuator relative displacement, relative velocity, absolute acceleration (actuator force for the active tendon system), and control effort.

$$\mathbf{J}_{1\text{-}5} = \text{diag}\left\{ \begin{matrix} [j_1 \quad j_1 \quad j_1]^{\mathrm{T}} \\ [j_2 \quad j_2 \quad j_2]^{\mathrm{T}} \\ [j_3 \quad j_4 \quad j_5]^{\mathrm{T}} \end{matrix} \right\}$$

$$\mathbf{Z}_{\mathrm{V}}^{\mathrm{AMD}} = \text{diag}\left\{ \begin{matrix} 0.51\frac{\mathrm{V}}{\mathrm{cm}}[1 \quad 1 \quad 1 \quad 1]^{\mathrm{T}} \\ 0.0204\frac{\mathrm{Vs}}{\mathrm{cm}}[1 \quad 1 \quad 1 \quad 1]^{\mathrm{T}} \\ \frac{\mathrm{V}}{g}[1 \quad 1 \quad 1 \quad 0.1]^{\mathrm{T}} \end{matrix} \right\}$$

$$\mathbf{Z}_{\mathrm{V}}^{\mathrm{TEN}} = \text{diag}\left\{ \begin{matrix} 0.25\frac{\mathrm{V}}{\mathrm{cm}}[1 \quad 1 \quad 1 \quad 31.48 \quad]^{\mathrm{T}} \\ 0.0102\frac{\mathrm{Vs}}{\mathrm{cm}}[1 \quad 1 \quad 1 \quad 38.627]^{\mathrm{T}} \\ 0.5\,\frac{\mathrm{V}}{g}[1 \quad 1 \quad 1 \quad 0.444\frac{g}{\mathrm{kN}}]^{\mathrm{T}} \end{matrix} \right\}$$

$$\mathbf{W}_{\mathbf{v}} = 0.01\sqrt{T}\,\mathbf{I} \qquad W_u = 1/\sigma_u^{\mathrm{MAX}}$$

$$\mathbf{M}_{\bar{\mathbf{z}}\mathbf{z}} = \begin{bmatrix} \begin{matrix} 1 & 0 & 0 & 0 \\ -1 & 1 & 0 & 0 \\ 0 & -1 & 1 & 0 \end{matrix} & \mathbf{0} & \mathbf{0} \\ \mathbf{0} & \mathbf{0} & \begin{matrix} 1 & 0 & 0 & 0 \\ 0 & 1 & 0 & 0 \\ 0 & 0 & 1 & 0 \end{matrix} \\ \begin{matrix} 0 & 0 & 0 & 1 \\ 0 & 0 & 0 & 0 \\ 0 & 0 & 0 & 0 \end{matrix} & \begin{matrix} 0 & 0 & 0 & 0 \\ 0 & 0 & 0 & 1 \\ 0 & 0 & 0 & 0 \end{matrix} & \begin{matrix} 0 & 0 & 0 & 0 \\ 0 & 0 & 0 & 0 \\ 0 & 0 & 0 & 1 \end{matrix} \end{bmatrix} \mathbf{Z}_{\mathrm{V}}^{-1} \tag{15}$$

H_2 Constraints

The benchmark requires that the root mean square controller output, actuator displacement, and actuator acceleration/force be less than critical values, to remain within the operational range of the actuator. This can be formulated as an H_2 constraint on the system shown in Fig. 4, where the new weights are given by

$$\mathbf{W}_{\mathbf{q}} = \begin{bmatrix} 1/\sigma_{\ddot{x}_m^a}^{\mathrm{MAX}} \text{ or } 1/\sigma_f^{\mathrm{MAX}} & 0 \\ 0 & 1/\sigma_{x_m}^{\mathrm{MAX}} \end{bmatrix} \quad \mathbf{q} = \begin{Bmatrix} \ddot{x}_m^a \text{ or } f \\ x_m \end{Bmatrix} \quad \mathbf{M}_{\underline{\mathbf{z}}\mathbf{z}} = \begin{bmatrix} 0 & 0 & 0 & 0 & 0 & 0 & 0 & 0 & 0 & 0 & 0 & 1 \\ 0 & 0 & 0 & 1 & 0 & 0 & 0 & 0 & 0 & 0 & 0 & 0 \end{bmatrix} \mathbf{Z}_{\mathrm{V}}^{-1} \tag{16}$$

and where $\mathbf{W}_{\underline{\mathbf{z}}}$ is a diagonal matrix to be determined for best performance. More properly, three H_2 constraints, one for each element of $\underline{\mathbf{z}}$ will be used herein (though one may substitute the single constraint in the interests of computational feasibility).

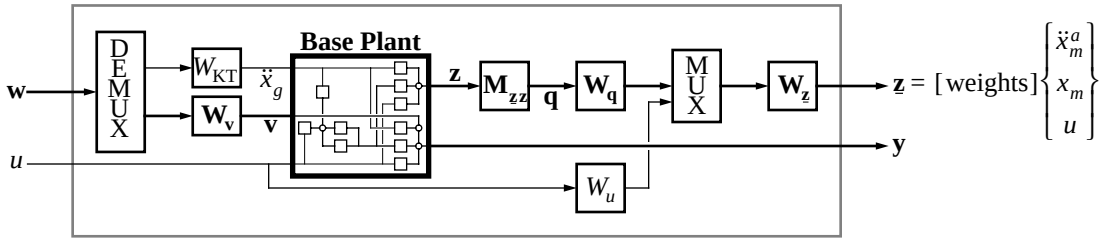

Figure 4. Block diagram of the H_2 constraints.

l_1 Constraints

The use of l_1 constraints permits the inclusion of the hard peak constraints of the actuator (to avoid saturation) as well as to facilitate bounding the performance of the peak response portion of the benchmark as measured via J_6 through J_{10}. The block diagram of the l_1 constraint subproblem is shown in Fig. 5, where the weights, chosen to reflect actuator peak constraints and the desired performance of the peak responses, are given by

$$W_{\mathbf{m}u} = \max_{\substack{\text{El Centro}\\ \text{Hachinohe}}} \left[\frac{\|\ddot{x}_g\|_\infty}{u^{\text{MAX}}} \right] \qquad \mathbf{J}_{6\text{-}10} = \min_{\substack{\text{El Centro}\\ \text{Hachinohe}}} \left[\frac{1}{\|\ddot{x}_g\|_\infty} \text{diag} \left\{ \begin{array}{c} [j_6 \quad j_6 \quad j_6]^{\text{T}} \\ [j_7 \quad j_7 \quad j_7]^{\text{T}} \\ \max(j_8, x_m^{\text{MAX}}) \\ j_9 \\ \max(j_{10}, \ddot{x}_m^{a\text{MAX}} \text{ or } f^{\text{MAX}}) \end{array} \right\} \right] \qquad (17)$$

$$\mathbf{M}_{\mathbf{mz}} = \begin{bmatrix} \mathbf{M}_{\bar{\mathbf{z}}\mathbf{z}} \\ \mathbf{M}_{\underline{\mathbf{z}}\mathbf{z}} \end{bmatrix}$$

The output vector $\bar{\mathbf{m}}$, the system responses whose peak magnitudes should be constrained or minimized, is the same as $\bar{\mathbf{z}}$ in the base H_2 problem but with different weights. The input r is the disturbance, which should be a bounded-magnitude signal for this subproblem (*i.e.*, in l_∞); the problem was studied with two input weights W_r: unity and a Kanai-Tajimi filter to more closely model earthquake input spectra (in which case r corresponds to the acceleration of bedrock in the Kanai-Tajimi earthquake model). The matrix $\mathbf{W_m}$ serves as a final scaling matrix and to select elements to include in the output vector $\mathbf{m}$.

It was observed in evaluation of several controllers that four of the ten elements of $\bar{\mathbf{m}}$ were critical (weighted measures of the 2nd and 3rd floor accelerations, $\bar{m}_5$ and $\bar{m}_6$; actuator velocity $\bar{m}_8$; and actuator acceleration/force $\bar{m}_{10}$); due to the expense of computing the l_1 norm and its gradient, the matrix $\mathbf{W_m}$ was used to select only those four outputs in $\mathbf{m}$ during the optimization.

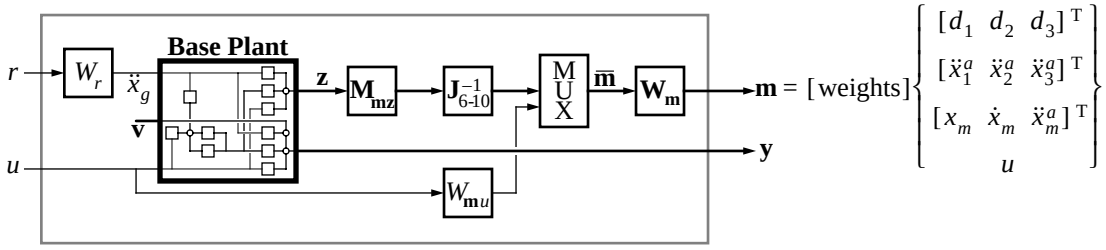

Figure 5. Block diagram of the l_1 constraints.

H_∞ Constraints

One typical purpose for involving H_∞ in many problems is to minimize the error in tracking given command inputs, generally by minimizing the weighted sensitivity of the system. The

problem at hand, however, is involved with augmenting the inherent damping in the structure. There is some concern that the nominal plant may not be entirely accurate, partly due to the inaccuracies involved with any model derived from experimental data, and partly due to the fact that high frequency dynamics (above 100 Hz for the AMD system, and above 50Hz for the TEN system) were truncated in forming the state-space model given in the benchmark problem. For this reason, a multiplicative uncertainty at the plant input is assumed, as seen in Fig. 6, with the dynamic weight $W_{e_1}(s) = \frac{3s^2 + 90s + 600}{s^2 + 300s + 30000}$ to account for the primarily high-frequency unmodeled dynamics, the 200 μs computational delay, and the input loop gain robustness requirement above 35Hz (15Hz was used for the TEN system). The resulting H_∞ constraint would be to include the "unmodelled dynamics" block in Fig. 6, where e_1 and d_1 and reflect the input and output of the unmodelled dynamics.

If taken by itself as an H_∞ control design problem, this H_∞ constraint has the trivial solution of the zero controller because the system is already stable, and the controller that minimizes the infinity norm of the transfer function from d_1 to e_1 is identically zero. This is not an inherent problem with the multiobjective problem, but for purposes of comparison, it is convenient to add an additional uncertainty block so that a base H_∞ controller can be designed. A robust performance control design problem can be solved using a fictitious uncertainty block, so such a block is placed at the plant output. The resulting design will not only be robustly stable, but its output performance should also be robust.

The weights for this additional block include the static diagonal weight $\mathbf{W}_{e_{2s}}$ and its inverse to normalize by the uncontrolled infinity norm for each channel, and the weight $\mathbf{W}_{e_2}$, which could be dynamic, but here will be set to identity.

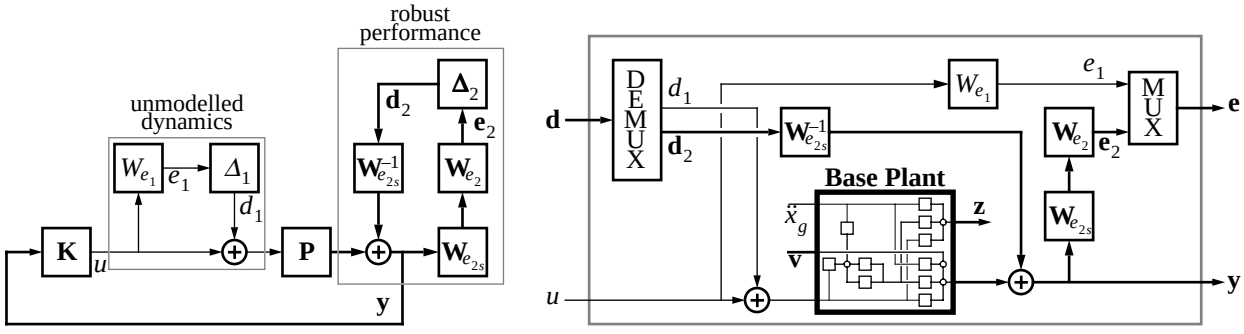

Figure 6. Block diagram of the H_∞ constraints.

Performance with Zero Controller

In order to properly judge superior control designs, the performance of the system with the "zero controller" (a 0V command signal always sent to the actuator) was first evaluated. Since the "closed-loop" system is linear, the RMS responses to the Kanai-Tajimi spectra can be efficiently computed by solving a Lyapunov equation (if a multi-input, single-output (MISO) system has Laplace transform $Y(s) = \mathbf{G}(s)\mathbf{W}(s)$, where $\mathbf{w}(t)$ is a zero-mean, Gaussian white noise vector process with $E[\mathbf{w}(t)\mathbf{w}^{\mathrm{T}}(s)] = \mathbf{I}\delta(t-s)$, then the expected output is $E[y^2(t)] = y_{\mathrm{RMS}}^2 = \|\mathbf{G}\|_2^2$). The peak responses to the known earthquakes can be simulated quickly via `lsim` in MATLAB®.

The resulting performance data are given in column #1 of Table IV (including the Kanai-Tajimi parameters ω_g and ζ_g that maximized the RMS values). For purposes of verification, the worst-case RMS and peak third-floor responses, used in the j_i performance weights, were computed and are shown in Table III; they are fairly consistent with the j_i given above in Table I.

Table III. Worst-case third-story responses with the zero controller

actuator	$\sigma_{x_3}^{\mathrm{worst}}$	$\sigma_{\dot{x}_3}^{\mathrm{worst}}$	$\sigma_{\ddot{x}_3^a}^{\mathrm{worst}}$	x_3^{worst}	$\dot{x}_3^{\mathrm{worst}}$	$\ddot{x}_3^{a\,\mathrm{worst}}$	earthquake
AMD	1.312911 cm ω_g=37.2674 $\frac{\mathrm{rads}}{\mathrm{sec}}$ ζ_g=0.30000	47.8787 $\frac{\mathrm{cm}}{\mathrm{sec}}$ ω_g=37.3078 $\frac{\mathrm{rads}}{\mathrm{sec}}$ ζ_g=0.30000	1.787342 g ω_g=37.3000 $\frac{\mathrm{rads}}{\mathrm{sec}}$ ζ_g=0.30000	3.444070 cm	131.3235 $\frac{\mathrm{cm}}{\mathrm{sec}}$	5.051008 g	El Centro
				1.662584 cm	58.6767 $\frac{\mathrm{cm}}{\mathrm{sec}}$	2.696785 g	Hachinohe
TEN	2.386049 cm ω_g=14.5478 $\frac{\mathrm{rads}}{\mathrm{sec}}$ ζ_g=0.30000	33.2794 $\frac{\mathrm{cm}}{\mathrm{sec}}$ ω_g=14.5764 $\frac{\mathrm{rads}}{\mathrm{sec}}$ ζ_g=0.30000	0.485246 g ω_g=14.5635 $\frac{\mathrm{rads}}{\mathrm{sec}}$ ζ_g=0.30000	6.574704 cm	99.9140 $\frac{\mathrm{cm}}{\mathrm{sec}}$	1.573521 g	El Centro
				3.850504 cm	56.0717 $\frac{\mathrm{cm}}{\mathrm{sec}}$	0.777907 g	Hachinohe

Performance with Sample Controller

In order to verify that the evaluation software was performing properly, the sample controller supplied with the benchmark proposal was evaluated. The results, shown in column #2 of Table IV, are consistent with those detailed in the benchmark and given above in Table II (with the exception of C_5, which in Table II may reflect just one of the two earthquakes in the benchmark), demonstrating that the evaluation software operates satisfactorily.

Base H_2 (LQG) Design

The primary parameter to be determined in a base H_2 design is the relative weight on the control effort, $W_{\ddot{\mathbf{z}}u}$. Full-order, discrete-time H_2-optimal controllers were computed using a wide

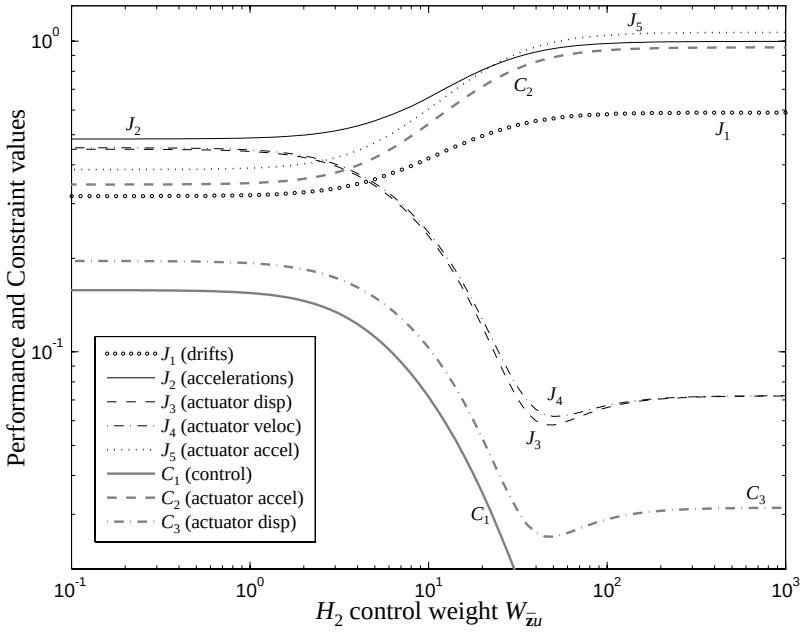

Figure 7. Control weight tradeoffs for the base H_2 controller in the AMD system.

range of control effort values to minimize $\|\mathbf{T}_{\bar{\mathbf{z}}\mathbf{w}}\|_2$. The resulting RMS performance and constraint values, assuming the system is sufficiently linear to apply the appropriate Lyapunov equations, are shown in Fig. 7. It is a worthwhile tradeoff to allow a larger control effort and greater actuator dynamics for the sake of reducing the larger performance and constraint values by letting $W_{\bar{z}u}$ be unity. A choice of $W_{\bar{z}u} < 1$ gains little in the way of the RMS performance and constraints, but may limit the ability to increase robustness and output magnitudes in subsequent optimization.

Two initial reduced order H_2 controllers were computed, one by a Hankel norm model reduction of the full H_2 controller, and the other by first reducing the plant and then designing an H_2 controller. These two designs were then used as initial conditions in a minimization of the H_2 norm of the closed loop formed with the full-order plant and the reduced-order controller. The performance on the benchmark for the resulting (reduced-order) H_2 optimal controller is given in column #3 of Table IV.

Two additional reduced-order controllers are used as starting points in the H_2/H_∞ optimization below, computed in a manner similar, but doing H_∞ control designs by minimizing $\|\mathbf{T}_{\mathbf{ed}}\|_\infty$.

The base H_2 problem contains somewhat conflicting goals, since the response of the structure and the response of the actuator cannot be simultaneously minimized. Figure 8 shows the tradeoff between the RMS structural response $\|\mathbf{T}^{\mathrm{Str}}_{\bar{\mathbf{z}}\mathbf{w}}\|_2$ (simply the first six outputs of $\bar{\mathbf{z}}$ in the base H_2

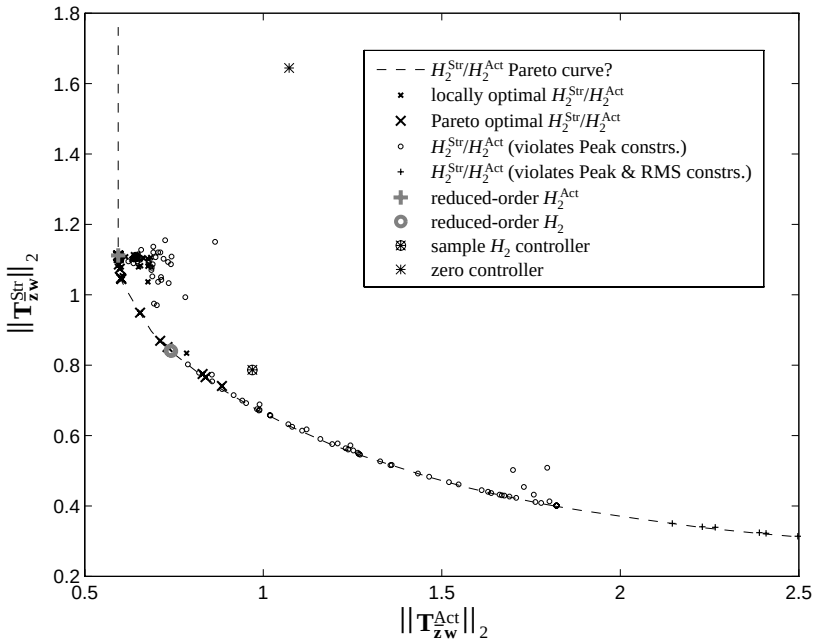

Figure 8. H_2^{Str}/H_2^{Act} tradeoffs between RMS structural and actuator responses for the AMD system.

plant) and the RMS actuator response $\|\mathbf{T}_{\mathbf{\bar{z}w}}^{Act}\|_2$ (the three actuator responses in $\mathbf{\bar{z}}$). (The constraints were ignored in the minimization, but are noted in the graph where violations occurred.) The benchmark performance of the controller that minimized the RMS actuator response is given in column #4 of Table IV, while column #5 gives the performance of the controller that minimized the RMS structural response while not violating RMS constraints (it did violate the peak active mass acceleration, but it is useful to see what the performance would be without the peak constraints). If the relative importance of these two sets of responses were known, one could appropriately weight the structural and actuator responses in the base H_2 problem; in the mixed-norm designs below, however, they are weighted equally.

Mixed H_2/H_∞ Design

About 100 different control designs were computed via the optimization software to study the tradeoffs between H_2 and H_∞ performance. The norms of the resulting closed-loop systems are plotted in Fig. 9; some of the designs obviously stalled at local minima, but a number of them demonstrate quite clearly that significant robust stability and robust performance can be obtained with near H_2 performance. (Note that the Pareto curve is approximate since the points from computed control designs are upper and right bounds on the curve, while constant lines at the closed-loop ∞-norm with the full-order H_∞ controller and the 2-norm with the H_2 controller are

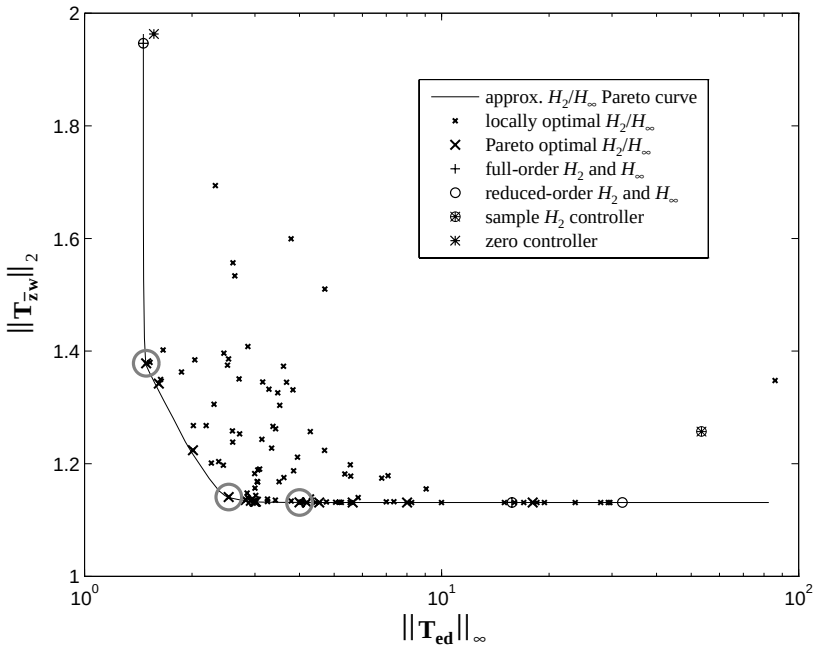

Figure 9. Pareto optimal curve for H_2/H_∞ AMD controllers.

left and lower bounds, respectively.) The two circled larger ×'s near the minimum H_2 have 2-norms only 0.86 and 0.015 percent above minimum, but at one thirteenth and one eighth of the infinity norm of the reduced-order H_2 optimal design. Such design points introduce significant robustness with negligible changes in RMS outputs to white noise excitation. The third circled large × has the opposite tradeoff, with a closed-loop infinity norm nearly that of the H_∞ optimal controller, but with a RMS output over 30% less.

The benchmark performance values for several of the (near-) Pareto optimal designs are graphed in Fig. 10, where it can be seen that the performance changes little for vast robustness improvements. The performance on the benchmark problem for the first of the above mentioned designs is given in column #6 of Table IV, and its input loop gain is shown in Fig. 11; this design far exceeds the robustness requirements in the benchmark description with little or no performance degradation. The performance of the controller resulting in the least mean square of the performance and constraint values (*i.e.*, $\arg\min_{\mathbf{K}} \sum_{i=1}^{10} J_i^2(\mathbf{K}) + \sum_{i=1}^{6} C_i^2(\mathbf{K})$) is given in column #7 of Table IV; this controller was one that significantly decreased the peak active mass acceleration.

If the robust performance component of the H_∞ constraint is removed, the resulting system has the zero controller as the H_∞ optimal robust controller. This complicates the characterization of the Pareto optimal tradeoff between the robust stability sensitivity, denoted here with $(\,)^{RS}$, and

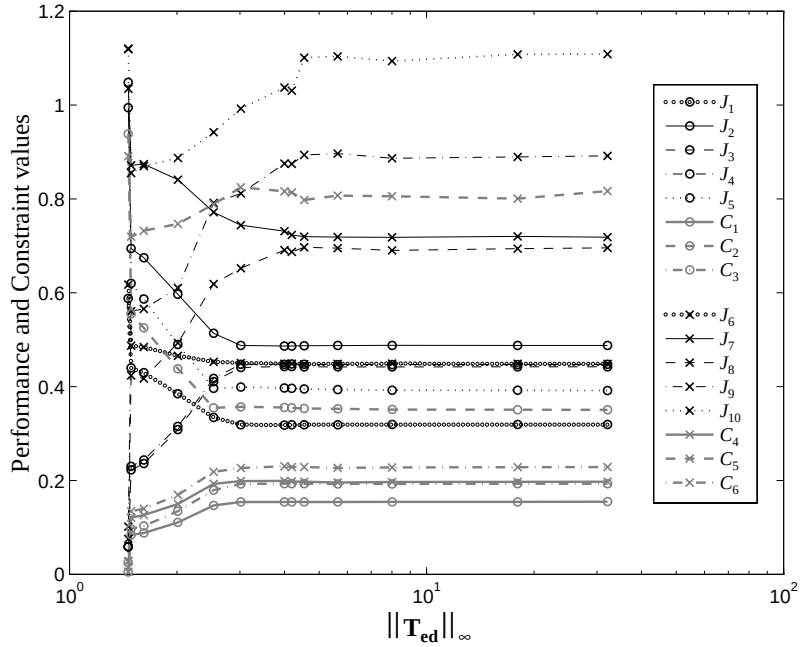

Figure 10. Linear performance and constraint values for (near-) Pareto H_2/H_∞ optimal AMD controllers.

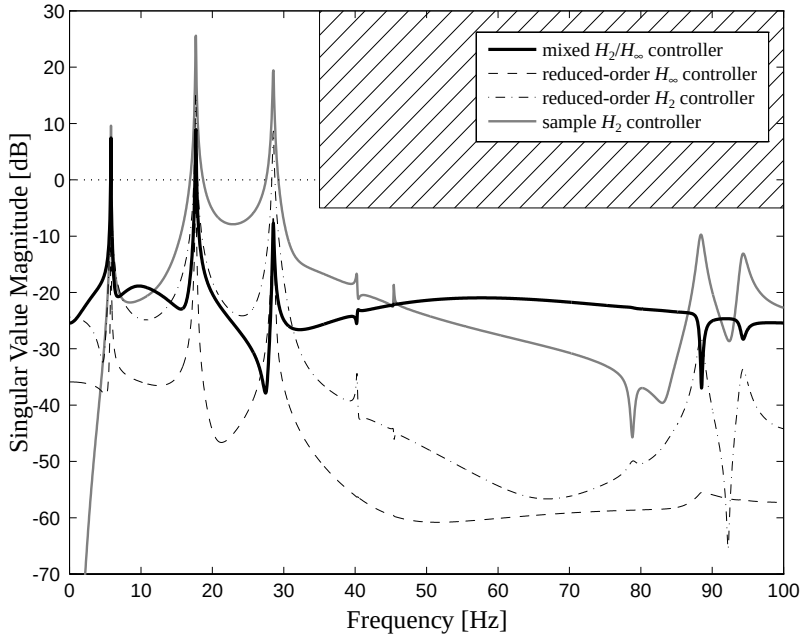

Figure 11. Input loop gain for a reduced-order H_2/H_∞ optimal controller for the AMD system.

the H_2 RMS response. Nevertheless, a number of mixed $H_2/H_\infty^{\mathrm{RS}}$ controllers were found as shown in Fig 12. The circled large $\times$ represents a controller that provides a closed-loop RMS output only 0.28% larger than the reduced-order H_2 optimal controller but 50 times as robust. The benchmark performance of this controller is given in column #8 of Table IV.

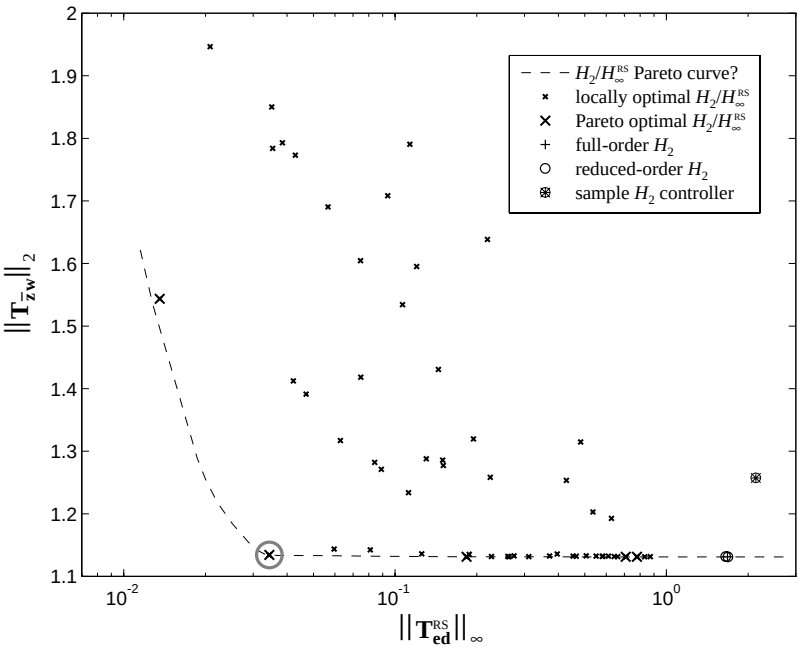

Figure 12. H_2/H_∞^{RS} RMS performance and robust stability sensitivity for the AMD system.

Mixed H_2/l_1 Design

The H_2/l_1 optimization problem is more difficult than the H_2/H_∞ for several reasons. First, computing the l_1 norm and its gradients with respect to controller parameters is quite expensive, limiting the number of trials that could be tested. The second is the lack of a good starting point; in the H_2/H_∞ design, it was observed that the optimization algorithm more readily relaxed constraints than restrict them, so using the H_∞ optimal controller as the starting point worked well. Here, the l_1 optimal controller was unknown; several semianalytical methods, including those of Khammash[12], were applied to solve for the l_1 optimal controller, but the combination of very low damping in some modes and high frequency actuator dynamics prevented a solution. Consequently, the optimization software was modified to do unconstrained l_1 optimization, which facilitated finding a number of controllers with smaller closed-loop l_1 norms (but with no knowledge of the proximity to the l_1 optimal controller).

Two different mixed H_2/l_1 strategies were attempted to determine if one or the other had an impact on the peak performance and constraint measures defined above. The first used the l_1 constraint with a constant weight on the input. About 40 mixed H_2/l_1 designs were computed and are shown in Fig. 13. The l_1 norm was reduced somewhat from the H_2 optimal controller, but not nearly as significantly as the H_∞ norm above. Some of these designs lowered the l_1 norm of the

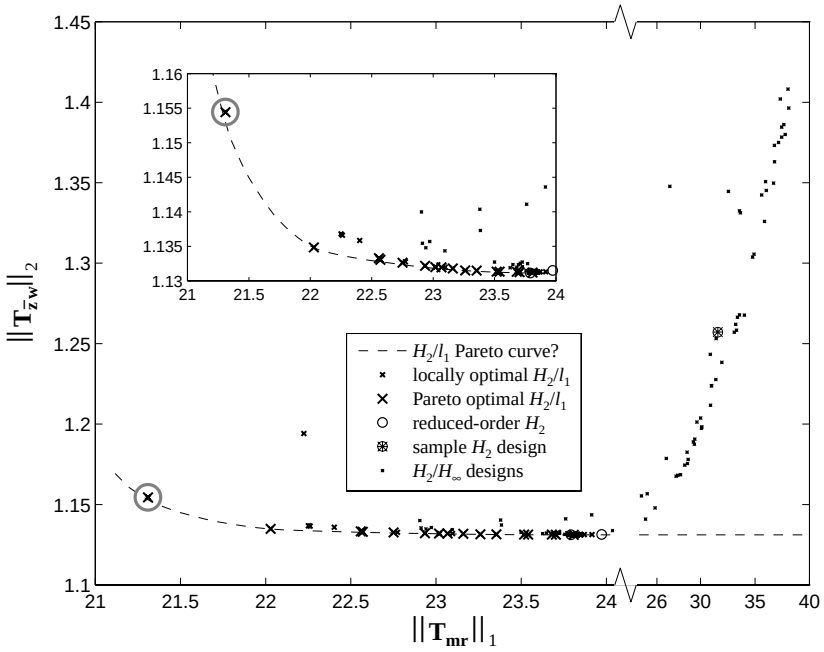

Figure 13. Mixed H_2/l_1 optimal controllers for the AMD system (no frequency dependent weight).

curve is poorly defined at the low l_1-norm end due to difficulties with local minima. The large circled $\times$ is the controller that obtained the smallest closed-loop l_1 norm.

The second set of mixed H_2/l_1 designs used a frequency-dependent input weight, that of the Kanai-Tajimi spectrum (with the ground frequency and damping that caused the worst response with the zero controller), to more closely model an earthquake record; to denote the frequency-dependent weight, these designs will be called H_2/l_1^{KT}. The results of the 55 H_2/l_1^{KT} designs are plotted in Fig. 14. The Pareto curve is a little better defined here, but without an optimal l_1 controller to give the lower bound, it is impossible to define the curve with much certainty. The results here are similar in that 5-10% drops in closed-loop l_1 norm can be achieved with only nominal sacrifice in H_2 performance.

Unfortunately, little correlation was found in the end between the closed-loop l_1 norm and the values of the peak performance J_{6-10} and constraint C_{4-6} values, as shown for the non-frequency-dependent H_2/l_1 designs in Fig. 15 over a range of the l_1 norm. The irregularity of the lines is to be expected, but the obvious lack of a general proportional trend between the l_1 norm and the performance/constraint values shows that the l_1 norm of the closed-loop cannot be used to predict peak responses to the known earthquake records.

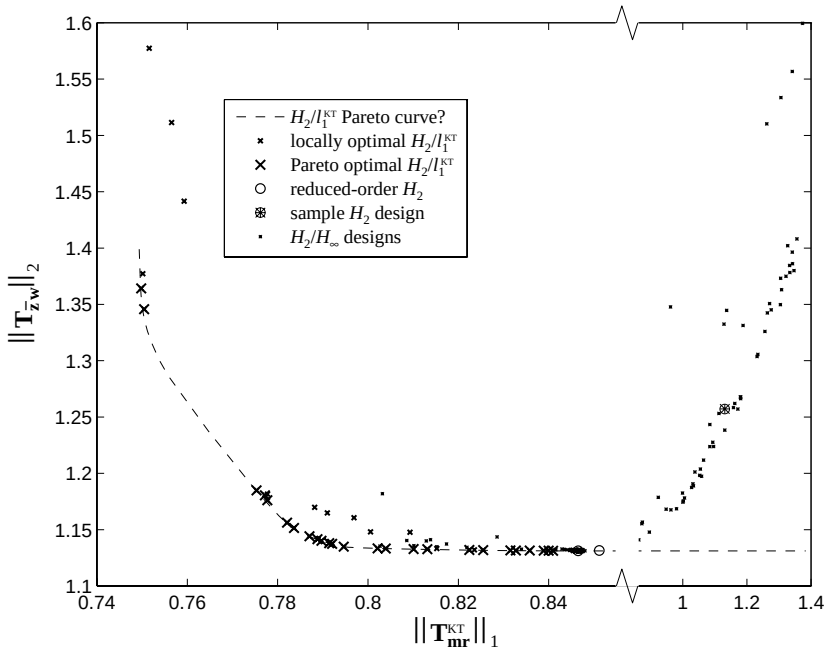

Figure 14. Mixed H_2/l_1^{KT} optimal controllers for the AMD system (Kanai-Tajimi frequency-dependent weight).

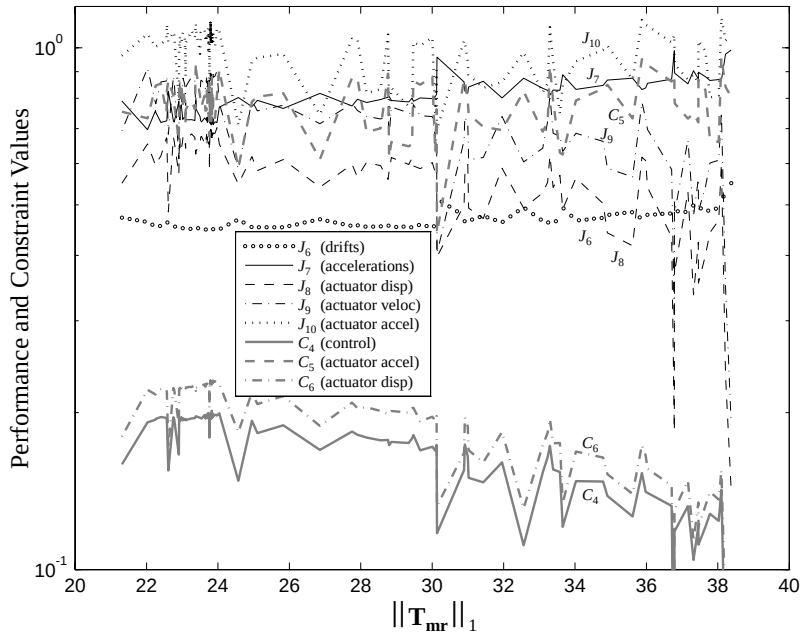

Figure 15. Peak linear performance and constraints are uncorrelated with closed-loop l_1 norm.

The lack of correlation was rather surprising at first, but, in retrospect, it makes some sense. The l_1 norm is the worst-case peak output over a very wide class of input excitations, those that are magnitude bounded (*i.e.*, those signals in l_∞), which includes persistent signals that have DC

offsets and long-term non-decaying behavior. The earthquake records used to evaluate the peak response of the closed-loop system for the benchmark, however, are finite in duration and more properly belong to the class of energy bounded signals (l_2). The worst case output magnitude over all possible energy-bounded inputs is governed by the H_2 norm of the system. Thus, the H_2 norm should be a better measure of peak output magnitudes than the l_1 norm for the excitations of interest here.

CONTROLLER DESIGNS: ACTIVE TENDON SYSTEM

Performance with Zero Controller

The performance of the active tendon system with the zero controller is given in column #9 of Table IV. This system has significantly tighter constraints, primarily on the actuator command voltage C_4 and actuator force C_5.

Base H_2 (LQG) Design

The analysis parallels that of the AMD system. The base H_2 tradeoff between performance and control effort is shown in Fig. 16. The control effort weight $W_{\bar{\mathbf{z}}u}$ has a very narrow admissible range since setting it to larger than 1.874 results in systems that violate the constraint on the

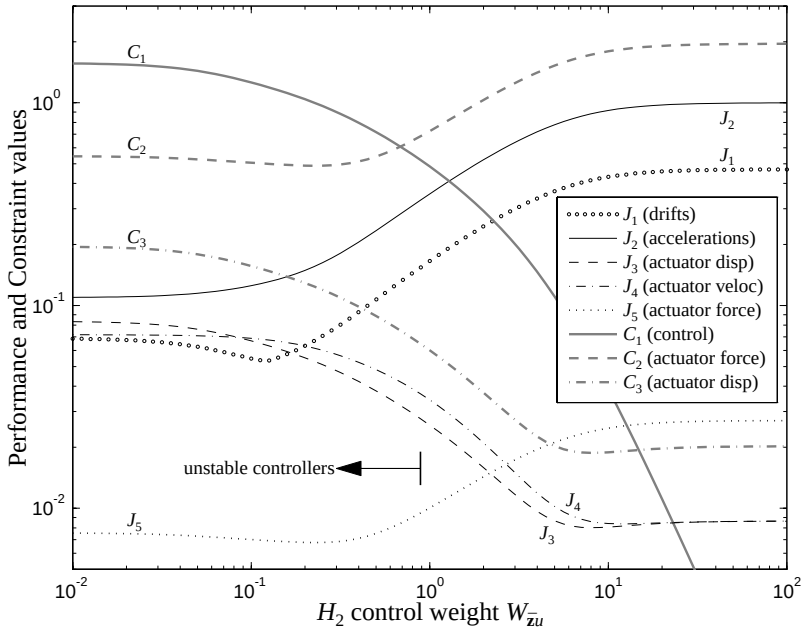

Figure 16. Control weight tradeoffs for the base H_2 controller in the TEN system.

actuator force ($C_2 > 1$), and for $W_{\bar{\mathbf{z}}u} < 0.887$, the resulting controller is unstable. Thus, the weight chosen here is again unity.

Several initial H_2 controllers, first full-order, then reduced order, were computed as described for the AMD system above; the resulting benchmark performance data for the best reduced-order H_2 design is given in column #10 of Table IV. It must be noted that the actuator velocity here reached its peak in a very different location in (ω_g, ζ_g) space than other RMS performance and constraint values. A reduced-order H_∞ optimal controller were also used as initial conditions for mixed optimization.

Mixed H_2/H_∞ Design

About 100 mixed H_2/H_∞ designs were computed to study the performance and robustness tradeoffs of the TEN system. The resulting norms are shown in Fig. 17; as was previously noted, the optimization algorithm does get stuck in local minima for many of these designs, but some are very good at improving robustness with little loss of the H_2 benefits. In fact, the H_2 optimal controllers have terrible robustness characteristics for the active tendon system. The circled large ×'s are controllers that generate closed-loop plants with 2-norms 1.2 and 0.1 percent larger than the H_2 optimal controller, but with infinity norms about 1/850th and 1/175th that of the H_2 controller. The input loop gains for these two designs are shown in Fig. 18 and the performance

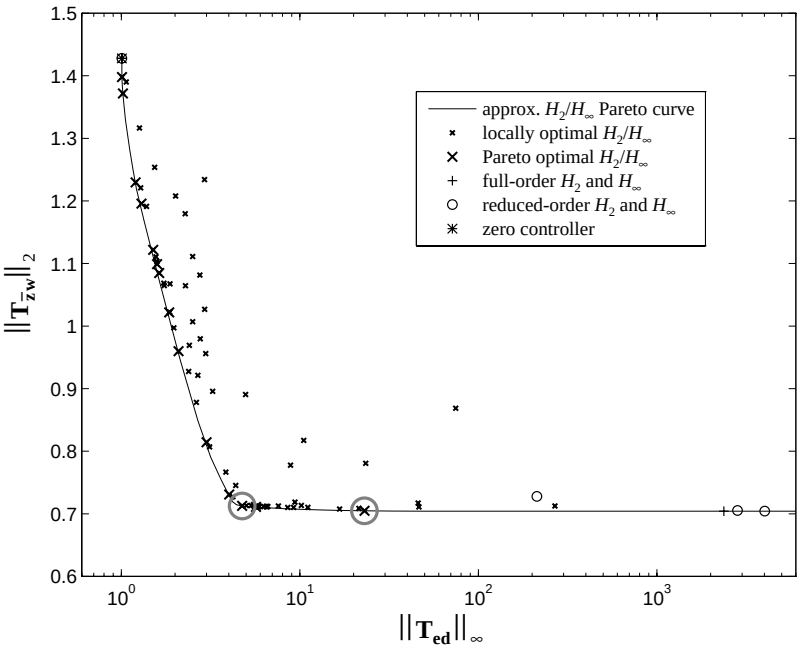

Figure 17. Pareto optimal curve for H_2/H_∞ TEN controllers.

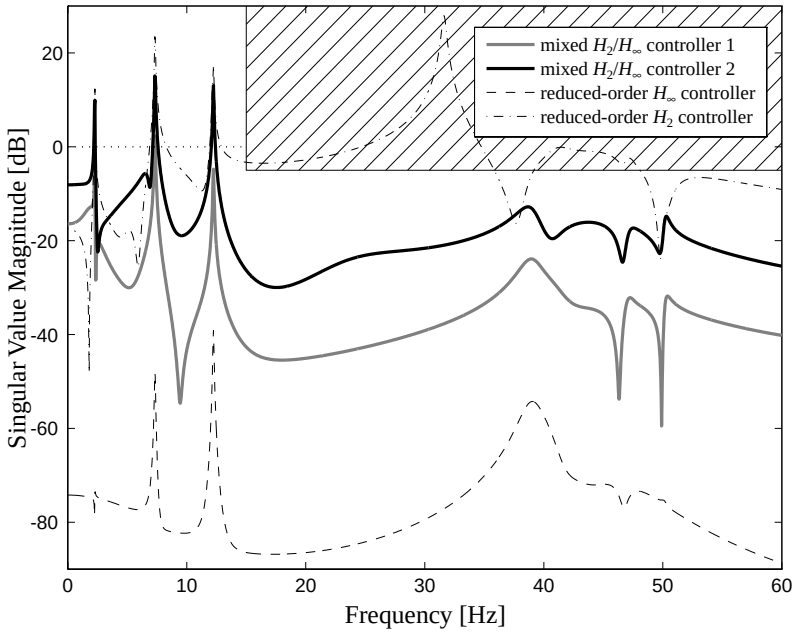

Figure 18. Input loop gain for reduced-order H_2/H_∞ optimal controller for the TEN system.

evaluation of the second is given in column #11 of Table IV. The optimal H_2 controller results in a fair sensitivity to high-frequency modelling errors that could, at worst, cause instability if the the truncated high-frequency modes dominate under some loading conditions. The mixed H_2/H_∞ designs, however, while retaining most of the RMS performance of the H_2 design, also capture some of the robustness of the H_∞ optimal controller.

Mixed H_2/l_1 Design

Due to the computational intensity and its inability to suppress peak responses of the AMD system, no mixed H_2/l_1 optimization was done on the active tendon system.

OBSERVATIONS AND CONCLUDING REMARKS

The mixed H_2/H_∞ optimal control design was able to provide controllers with significantly greater robustness characteristics at little cost to RMS and peak performance measures defined in the benchmark. This was especially noticeable in the active tendon system, where the infinity-norms of the H_2 optimal controllers were quite large. The robustness was a relatively minor point in the benchmark definition, but it is a critical safety issue for actively-controlled buildings and must be included in an evaluation of controller design.

The performance of the controllers mentioned herein is generally better than the sample controller provided with the benchmark, though the definition of "better" is, of course, rather application specific and will vary with the requirements of the structure. The 50 "best" AMD results here averaged about 20% less than the sample controller (where all 10 performance measures and the 6 weighted constraints are averaged together), with the best being 28% less.

The computer resources required for the multiobjective optimizations performed for this study vary significantly depending on what objective and constraint functions are used. The l_1 norms were routinely significantly more computationally intensive than the others, up to the better part of a day of CPU time on an HP9000/780 workstation. Other mixed-norm designs, such as the RMS structural/actuator response tradeoffs, generally took only a few minutes on the same platform. A full Simulink® simulation (up to 300 seconds) of one Kanai-Tajimi spectrum for one controller took about 105 minutes, so the evaluation was at least as expensive as the design process.

It was observed in the process of doing H_2/H_∞ mixed designs that the optimization algorithm more readily relaxed constraints than restricted them, being less likely to get stuck at local minima. For example, in an H_2/H_∞ problem, starting with an H_∞ optimal controller and relaxing the constraint often results in solutions that are closer to the Pareto optimal curve than starting with a controller that is closer to H_2 optimal and searching for a more constrained H_∞ value.

It may be noted that the H_∞ portion of the problem tends toward the conservative side since the overall uncertainty is structured due to the two separate uncertainty blocks. Walker and Ridgely[16] have done some work in mixed H_2/μ optimization, so the above development could replace the H_∞ constraint with a μ constraint to more closely model the true system uncertainty.

Investigation into l_1 optimization in the mixed-norm context for this benchmark proved inadequate for reducing peak responses and accommodating peak hardware constraints. Since an earthquake is generally an energy-bounded excitation (it dies out after a short time), the l_1 norm might not be the best induced norm to use since that assumes the input to be in too broad a class of signals (l_∞). (In fact, it may be argued that an earthquake excitation is in l_1, an even narrower class of signals whose l_1 norm is bounded.) The H_2 norm, already included for minimizing RMS response, has a bigger impact on peak outputs to the real earthquake records than did controllers with small corresponding l_1 norms.

This study demonstrates the usefulness of mixed-norm optimization to allow the control designer to dramatically improve robustness while retaining the performance of H_2/LQG optimal controllers. Understanding these tradeoffs is essential to the control design process.

Table IV. Performance and constraints of the AMD and TEN systems with various controllers.
The worst case (ω_g,ζ_g) locations were found for each RMS value, using 300 (AMD) or 750 (TEN) seconds of response to a Kanai-Tajimi excitation, and are given below the corresponding J and C values (ω_g is in rads/sec).

	1	2	3	4	5	6	7	8	9	10	11
Sys:	**AMD**	**AMD**	**AMD**	**AMD**	**AMD**	**AMD**	**AMD**	**AMD**	**TEN**	**TEN**	**TEN**
Name:	Zero	SampleH_2	Base H_2	H_2^{Act}	H_2^{Str}	H_2/H_∞ #1	H_2/H_∞ #2	H_2/H_∞^{RS}	Zero	Base H_2	H_2/H_∞
Note:		min. accel. responses	min. struct. & actuator responses	min. actuator responses	min. structural responses	stability/ perform. robustness	least mean sq. perf. & cnstr. vals	stability robustness		min. struct. & actuator responses	stability/ perform. robustness
J_1	0.589235 ω_g=37.2604 ζ_g=0.30000	0.284008 ω_g=37.1276 ζ_g=0.30000	0.331097 ω_g=37.2728 ζ_g=0.30000	0.398656 ω_g=37.3087 ζ_g=0.30000	0.148870 ω_g=36.8128 ζ_g=0.30000	0.327632 ω_g=37.2682 ζ_g=0.30000	0.324451 ω_g=37.2665 ζ_g=0.30000	0.313034 ω_g=37.2563 ζ_g=0.30000	0.469652 ω_g=14.5492 ζ_g=0.30000	0.167053 ω_g=14.4392 ζ_g=0.30000	0.167236 ω_g=14.4387 ζ_g=0.30000
J_2	0.998515 ω_g=37.3000 ζ_g=0.30000	0.439718 ω_g=37.0922 ζ_g=0.30000	0.476400 ω_g=37.2648 ζ_g=0.30000	0.632393 ω_g=37.4397 ζ_g=0.30000	0.221632 ω_g=36.5708 ζ_g=0.30000	0.503912 ω_g=37.2700 ζ_g=0.30000	0.498581 ω_g=37.2628 ζ_g=0.30000	0.479473 ω_g=37.2476 ζ_g=0.30000	1.000507 ω_g=14.5635 ζ_g=0.30000	0.359133 ω_g=14.4931 ζ_g=0.30000	0.359519 ω_g=14.4929 ζ_g=0.30000
J_3	0.072189 ω_g=37.2522 ζ_g=0.30000	0.511574 ω_g=37.0152 ζ_g=0.30000	0.435891 ω_g=37.2366 ζ_g=0.30000	0.283548 ω_g=37.3355 ζ_g=0.30000	1.072474 ω_g=36.3575 ζ_g=0.30000	0.404407 ω_g=37.3585 ζ_g=0.30000	0.398811 ω_g=37.2862 ζ_g=0.30000	0.433318 ω_g=37.2743 ζ_g=0.30000	0.008641 ω_g=14.5400 ζ_g=0.30000	0.025988 ω_g=14.7564 ζ_g=0.30000	0.025956 ω_g=14.7542 ζ_g=0.30000
J_4	0.082320 ω_g=37.4052 ζ_g=0.30000	0.512567 ω_g=37.1222 ζ_g=0.30000	0.440530 ω_g=37.4334 ζ_g=0.30000	0.288202 ω_g=37.4246 ζ_g=0.30000	1.047233 ω_g=37.4442 ζ_g=0.30000	0.410838 ω_g=37.5295 ζ_g=0.30000	0.403989 ω_g=37.3699 ζ_g=0.30000	0.438351 ω_g=37.4553 ζ_g=0.30000	0.008651 ω_g=14.5763 ζ_g=0.30000	0.065933 ω_g=50.0000 ζ_g=0.75000	0.061770 ω_g=50.0000 ζ_g=0.75000
J_5	1.067546 ω_g=37.3060 ζ_g=0.30000	0.626813 ω_g=37.0076 ζ_g=0.30000	0.368803 ω_g=37.9657 ζ_g=0.30000	0.389057 ω_g=37.2734 ζ_g=0.30000	1.056882 ω_g=38.6359 ζ_g=0.30000	0.366769 ω_g=37.8947 ζ_g=0.30000	0.402087 ω_g=37.2931 ζ_g=0.30000	0.370105 ω_g=38.1447 ζ_g=0.30000	0.027074 ω_g=14.5386 ζ_g=0.30000	0.010131 ω_g=14.2808 ζ_g=0.30000	0.010132 ω_g=14.2813 ζ_g=0.30000
J_6	0.620058	0.455587	0.449376	0.912614	0.356579	0.453735	0.469161	0.448668	0.478946	0.294108	0.298966
J_7	0.717755	0.710194	0.715053	0.710194	0.559262	0.770059	0.805363	0.749228	0.822220	0.775928	0.771151
J_8	0.077206	0.667990	0.689468	0.397785	3.159213	0.621133	0.547477	0.687785	0.009316	0.057316	0.057130
J_9	0.083293	0.775300	0.880412	0.445912	3.264125	0.783109	0.586780	0.954007	0.010837	0.203174	0.184940
J_{10}	1.142254	1.336047	1.031068	0.513109	4.533990	0.858705	0.682718	1.156828	0.079961	0.040999	0.039997
C_1	0	0.143045 ω_g=37.1436 ζ_g=0.30000	0.147656 ω_g=37.5456 ζ_g=0.30000	0.110122 ω_g=37.6263 ζ_g=0.30000	0.365361 ω_g=36.7604 ζ_g=0.30000	0.140550 ω_g=37.6811 ζ_g=0.30000	0.127599 ω_g=37.5930 ζ_g=0.30000	0.146899 ω_g=37.5627 ζ_g=0.30000	0	0.490599 ω_g=14.6978 ζ_g=0.30000	0.490159 ω_g=14.6972 ζ_g=0.30000
C_2	0.955454 ω_g=37.3060 ζ_g=0.30000	0.560998 ω_g=37.0076 ζ_g=0.30000	0.330079 ω_g=37.9657 ζ_g=0.30000	0.348206 ω_g=37.2734 ζ_g=0.30000	0.945909 ω_g=38.6359 ζ_g=0.30000	0.328258 ω_g=37.8947 ζ_g=0.30000	0.359868 ω_g=37.2931 ζ_g=0.30000	0.331244 ω_g=38.1447 ζ_g=0.30000	*1.956081* ω_g=14.5386 ζ_g=0.30000	0.732025 ω_g=14.2808 ζ_g=0.30000	0.732070 ω_g=14.2813 ζ_g=0.30000
C_3	0.031522 ω_g=37.2522 ζ_g=0.30000	0.223387 ω_g=37.0152 ζ_g=0.30000	0.190339 ω_g=37.2366 ζ_g=0.30000	0.123816 ω_g=37.3355 ζ_g=0.30000	0.468313 ω_g=36.3575 ζ_g=0.30000	0.176591 ω_g=37.3585 ζ_g=0.30000	0.174147 ω_g=37.2862 ζ_g=0.30000	0.189215 ω_g=37.2743 ζ_g=0.30000	0.020219 ω_g=14.5400 ζ_g=0.30000	0.060813 ω_g=14.7564 ζ_g=0.30000	0.060737 ω_g=14.7542 ζ_g=0.30000
C_4	0	0.175165	0.196315	0.116033	0.514544	0.190882	0.145384	0.200995	0	0.947226	0.951560
C_5	0.905539	0.804580	0.705785	0.431867	*2.824588*	0.722743	0.574621	0.774253	*1.925718*	0.987402	0.963263
C_6	0.027950	0.224130	0.225663	0.131725	0.582699	0.216185	0.181141	0.231494	0.020030	0.120719	0.122831

The controllers mentioned herein are available upon request.

The authors would like to acknowledge and thank Prof. D.B. Ridgely and his colleagues for making the MXTOOLS toolbox available for our use.

REFERENCES

1. B.F. Spencer, Jr., S.J. Dyke, and H.S. Deoskar. "Benchmark Problems in Structural Control — Part I: Active Mass Driver System." *Earthquake Engineering and Structural Dynamics*, to appear in 1997.
2. B.F. Spencer, Jr., S.J. Dyke, and H.S. Deoskar. "Benchmark Problems in Structural Control — Part II: Active Tendon System." *Earthquake Engineering and Structural Dynamics*, to appear in 1997.
3. L.L. Chung, R.C. Lin, T.T. Soong, and A.M. Reinhorn. "Experiments on Active Control for MDOF Seismic Structures." *Journal of Engineering Mechanics*, ASCE, **115**(8), 1609-1627.
4. P.P. Khargonekar and M.A. Rotea. "Mixed H_2/H_∞ Control: A Convex Optimization Approach." *IEEE Transactions on Automatic Control*, **36**(7), July 1991, 824-837.
5. I. Kaminer, P.P. Khargonekar, and M.A. Rotea. "Mixed H_2/H_∞ Control for Discrete-time Systems via Convex Optimization." *Automatica*, **29**(1), 1993, 57-70.
6. D.S. Bernstein and W.M. Haddad. "LQG Control with an H_∞ Performance Bound: A Riccati Equation Approach." *IEEE Transactions on Automatic Control*, **34**(3), March 1989, 293-305.
7. J.C. Doyle, K. Glover, P.P. Khargonekar, and B.A. Francis. "State-Space Solutions to Standard H_2 and H_∞ Control Problems." *IEEE Transactions on Automatic Control*, **34**(8), Aug. 1989, 831-847.
8. K. Glover and J.C. Doyle. "State-Space Formulae for all Stabilizing Controllers that Satisfy an H_∞ Norm Bound and Relations to Risk Sensitivity." *Systems and Control Letters*, 11(2), Aug. 1988, 167-172.
9. G.J. Balas, J.C. Doyle, K. Glover, A. Packard, and R. Smith. *μ-Analysis and Synthesis Toolbox: User's Guide*, version 3.0, The MathWorks, Inc., Natick, Mass. and MUSYN, Inc., Minneapolis, 1995.
10. M.A. Dahleh and J.B. Pearson. "l_1 Optimal Feedback Controllers for MIMO Discrete-time Systems." *IEEE Transactions on Automatic Control*, **32**(4), April 1987, 314-322.
11. M.A. Dahleh and I.J. Diaz-Bobillo. *Control of Uncertain Systems: a linear programming approach*, Prentice Hall, Englewood Cliffs, 1995.
12. M.H. Khammash. "Synthesis of Globally Optimal Controllers for Robust Performance to Unstructured Uncertainty." *IEEE Transactions on Automatic Control*, **41**(2), Feb. 1996, 189-198.
13. M. Whorton, H. Buschek, and A.J. Calise. "Homotopy Algorithm for Fixed Order Mixed H_2/H_∞ Design." *Journal of Guidance, Control, and Dynamics*, **19**(6), Nov.-Dec. 1996, 1262-1296.
14. P.G. Voulgaris. "Optimal H_2/l_1 Control via Duality Theory." *IEEE Transactions on Automatic Control*, **40**(11), Nov. 1995, 1881-1888.
15. J.C. Ullauri, D.E. Walker, and D.B. Ridgely. "Reduced Order Mixed H_2/H_∞ Optimization with Multiple H_∞ Constraints." *1994 AIAA Guidance, Navigation, and Control Conference*, Scottsdale, AZ, Aug. 1-3, 1994. AIAA-94-3658-CP. Proceedings (vol. 3), 1051-1060.
16. D.E. Walker and D.B. Ridgely. "Mixed H_2/μ Optimization." *Automatic Control in Aerospace 1994* (D.B. Schaechter and K.R. Lorell, eds.; IFAC Symposium on Automatic Control in Aerospace, Palo Alto, CA, Sept. 12-16, 1994), Pergamon/IFAC, Oxford, 1995, 431-436.
17. D.R. Jacques, D.B. Ridgely, and R.A. Canfield. "Discrete-Time, Mixed-Norm Control Synthesis Applied to Aircraft Terrain Following." *Journal of Guidance, Control, and Dynamics*, **19**(5), Sept.-Oct. 1996, 1088-1094.
18. D.R. Jacques, R.A. Canfield, D.B. Ridgely, and M.S. Spillman. "A MATLAB Toolbox for Fixed-Order, Mixed-Norm Control Synthesis." *IEEE Control Systems Magazine*, **16**(5), Oct. 1996, 36-44.
19. D.R. Jacques, R.A. Canfield, and D.B. Ridgely. "MXTOOLS: A MATLAB® Toolbox for Fixed Order, Mixed-Norm Control Synthesis." MXTOOLS code and documentation in `ftp://dream.afit.af.mil/pub/matlab/`, 1995.
20. B.F. Spencer, Jr. "Structural Dynamics and Control / Earthquake Engineering Laboratory: Benchmark Problem." Web page at `http://www.nd.edu/~quake/docs/benchmark.html`, 1996.
21. T.T. Soong and M. Grigoriu. *Random Vibration of Mechanical and Structural Systems*, Prentice Hall, Englewood Cliffs, NJ, 1993.
22. A. Grace. *Optimization Toolbox*, The MathWorks, Inc., Natick, Mass., 1992.
23. G.H. Golub and C.F. Van Loan. *Matrix Computations* (2nd ed.), Johns Hopkins University Press, Baltimore, 1989, 557*ff*.